Plasma-Structured Molybdenum Oxycarbides Enabling Ultrastable Acidic Hydrogen Evolution up to 10 A cm^{-2}

Shiwen Wu[1, †], Taesoon Hwang[2, †], Amirarsalan Mashhadian[1], Tianyi Li[3], Kyeongjae Cho[2,*], Guoping Xiong[1,*]

[1.] Department of Mechanical Engineering, The University of Texas at Dallas, Richardson, Texas 75080, USA

[2.] Department of Material Science Engineering, The University of Texas at Dallas, Richardson, Texas 75080, USA

[3.] X-ray Science Division, Argonne National Laboratory, 9700 South Cass Avenue, Lemont, IL, 60439, United States

† Shiwen Wu and Taesoon Hwang contribute equally

* Corresponding authors: Kyeongjae Cho: kjcho@utdallas.edu; Guoping Xiong: guoping.xiong@utdallas.edu

Abstract

Fabricating electrocatalysts capable of stable operation at high current densities is crucial for the industrial proton exchange membrane water electrolysis. However, current catalysts suffer from high overpotentials and rapid degradation when working in acid electrolytes at high current densities. In this paper, we report the design of vertical-standing, nanoedge-enriched molybdenum oxycarbide electrocatalysts via plasma-enhanced chemical vapor deposition (PECVD) with salts as precursors to achieve outstanding acidic electrocatalytic hydrogen evolution performance. Benefiting from their unique structural features and chemical compositions, the plasma-grown molybdenum oxycarbide catalysts exhibit a low overpotential of 415 mV at industrial-level high current densities up to 10 A cm^{-2} for 1,000 h, corresponding to an ultrahigh hydrogen throughput of 4,477.4 L cm^{-2} and substantially surpassing the performance of state-of-the-art transition metal- and even noble metal-based catalysts. This work paves the way for the development of new transition metal-based catalysts for practical industrial electrocatalytic hydrogen evolution.

Keywords

Plasma-enhanced chemical vapor deposition; molybdenum oxycarbide; electrocatalytic hydrogen evolution; industrial-level current density; ultrasharp edges

Electrochemical water splitting offers a cost-effective and promising approach for producing clean hydrogen with high purity through the hydrogen evolution reaction (HER)[1–3]. For practical industrial applications, developing electrocatalysts that can maintain low overpotentials and extend operational durations at high current densities is essential. For instance, the U.S. Department of Energy (DOE) has set an aggressive target for proton-exchange-membrane water electrolysis[4], including a high current density of 3 A cm^{-2} and a degradation rate of 0.13% over 1,000 h. HER conducted in acidic electrolytes is more efficient than alkaline electrolysis because of its higher energy efficiency, greater achievable current densities, and reduced gas crossover[5,6]. Despite these advantages, critical challenges still exist in designing efficient catalysts for HER in acidic electrolytes at high current densities: 1) Poor long-term stability. The corrosive environment of strong acids, combined with the heat and mechanical stresses from hydrogen (H_2) bubble generation at high current densities, severely challenges the stability of existing catalysts, including those noble metal-based ones[7–9]. Catalysts with both excellent thermodynamic stability and robust physical adhesion to substrates are required to ensure long-term stability under these harsh conditions. 2) High overpotential at large current densities. At high current densities, high activation energy is required to drive HER because of the rapidly consumed H_3O^+ near the catalyst surface[10,11] and the blocked active sites by the high-level H_2 bubble coverage at catalyst surfaces[12–15], leading to increased overpotential and reduced energy efficiency.

Non-precious transition metal-based electrocatalysts, including transition metal oxides[16,17], carbides[18,19], and sulfides[20,21], have emerged as promising alternatives to noble platinum (Pt)-based catalysts for HER. However, the existing transition metal-based catalysts generally exhibit optimal activities only at low current densities (1-100 mA cm^{-2}) with limited stability, making their operation in acidic electrolytes at industrial-level current densities (> 3 A cm^{-2}) quite challenging. Non-equilibrium plasmas, characterized by highly energetic reactive species in a far-from-equilibrium state and the capability to operate at low temperatures, offer distinct advantages in the development and fabrication of innovative materials[22–24]. The existence of non-equilibrium plasmas can significantly influence nucleation and crystal growth processes in material synthesis, facilitating thermodynamically unfavorable reactions that are difficult or impossible to achieve using conventional equilibrium thermal methods[24,25]. Consequently, plasma-assisted fabrication methods hold great promise for developing novel transition metal-based compounds with specifically tailored morphologies and chemical compositions to achieve high-performance hydrogen evolution at industrial-level current densities.

In this paper, we report the *in-situ* growth of vertically standing nanoedge-enriched molybdenum oxycarbide nanosheets (MoO_xC_y) through plasma-enhanced chemical vapor deposition (PECVD) based on salts as precursors to achieve ultrahigh-throughput acidic electrocatalytic hydrogen evolution at high current densities up to 10 A cm^{-2}. The plasma-structured nanoedge-enriched MoO_xC_y catalysts offer the following benefits toward HER: 1) Significantly improved thermodynamic stability of catalysts because of the non-equilibrium plasma-engineered structures, which are kinetically unfavorable to obtain through conventional equilibrium thermal methods; 2) Strong localized electric field near the ultrasharp edges of the catalysts, enabling fast diffusion of H_3O^+ from the electrolyte to catalyst surface; 3) Efficient hydrogen bubble detachment from the nanoedge-enriched structure with high roughness, maintaining continuous exposure of catalytic sites to the surrounding electrolyte. Benefiting from the unique plasma-induced morphology and chemical composition, the MoO_xC_y exhibits outstanding HER performance with a low overpotential (η) of 415 mV at an ultrahigh current density (j) of up to 10 A cm^{-2} for 1,000 h in 0.5 M H_2SO_4. This performance leads to an ultrahigh H_2 throughput of 4,477.4 L cm^{-2}, substantially outperforming the state-of-the-art transition metal- and even noble metal-based catalysts. This work paves new avenues for the development of high-efficiency catalysts for practical industrial applications in electrocatalytic hydrogen evolution.

Synthesis and characterization of the MoO_xC_y catalyst

The vertically standing, nanoedge-enriched MoO_xC_y arrays were synthesized through a PECVD process with a salt mixture of earth-abundant MoO_3 and NaCl as the solid precursors (see details in Supplementary Materials). Firstly, MoO_xC_y arrays were directly grown on carbon cloth substrates in a non-equilibrium hydrogen plasma environment within 20 min, denoted as HP-MoOC. During the growth process, the mixture of MoO_3 and NaCl powders were introduced in the upstream of the substrates inside the tube (Figure 1a) to generate volatile metal oxychlorides (i.e., MoO_2Cl_2) at elevated temperatures as the metal precursor[26–28]:

$$MoO_3(s) + 2NaCl(s) \rightarrow MoO_2Cl_2(g) + Na_2MoO_4(l) \tag{1}$$

The gaseous MoO_2Cl_2 was subsequently guided to the carbon cloth substrate, promoting the growth of MoO_xC_y within the highly reductive hydrogen plasma environment. Meanwhile, the surface of carbon fiber substrates was etched by hydrogen plasma, generating hydrocarbon species[29,30] that served as the carbon source for MoO_xC_y formation. Moreover, the presence of a strong electric field in the plasma sheath can guide the growth of materials in a vertical orientation to the substrate[31]. As shown in Figure 1b, the PECVD-grown HP-MoOC exhibits unique petal-like structures, with MoO_xC_y nanosheets aligned roughly perpendicularly to the substrate, exhibiting high aspect ratios and abundant exposed ultrasharp nanoedges. The thickness of the nanosheets is only a few nanometers (Supplementary Figure S2). Such morphology distinctly differs from the particle- or flat sheet-like transition metal oxides that are grown by conventional thermal chemical vapor deposition reported in prior studies[26,27,32]. The chemical composition of HP-MoOC was determined using energy-dispersive X-ray spectroscopy (EDX) on the cross-section of the MoO_xC_y sheets, revealing a Mo:O:C atomic ratio of approximately 1:1:1 (Supplementary Figure S3). For comparison, control samples (denoted as HP-MoO_2) were fabricated under the same PECVD growth conditions but using nickel foam as the substrate. Although these samples share a similar morphology with HP-MoOC, their chemical composition is markedly different, containing only Mo and O (Supplementary Figure S4). This difference is attributed to the lack of carbon resources in the growth environment, leading to the formation of molybdenum oxide rather than oxycarbide.

The carbon content in HP-MoOC was further increased through additional methane plasma treatment during PECVD (see details in Supplementary Materials). The resulting product was denoted as HCP-MoOC and still maintained the nanoedge-enriched morphology (Figure 1c). The vertically standing morphology of HCP-MoOC was verified through the cross-sectional scanning electron microscope (SEM) image (Figure 1d), and the elemental mappings obtained by EDX confirmed the uniform distribution of Mo, C, and O elements within the HCP-MoOC. The Mo:O:C atomic ratio of HCP-MoOC was determined to be 1:1:3

(Supplementary Figure S5).

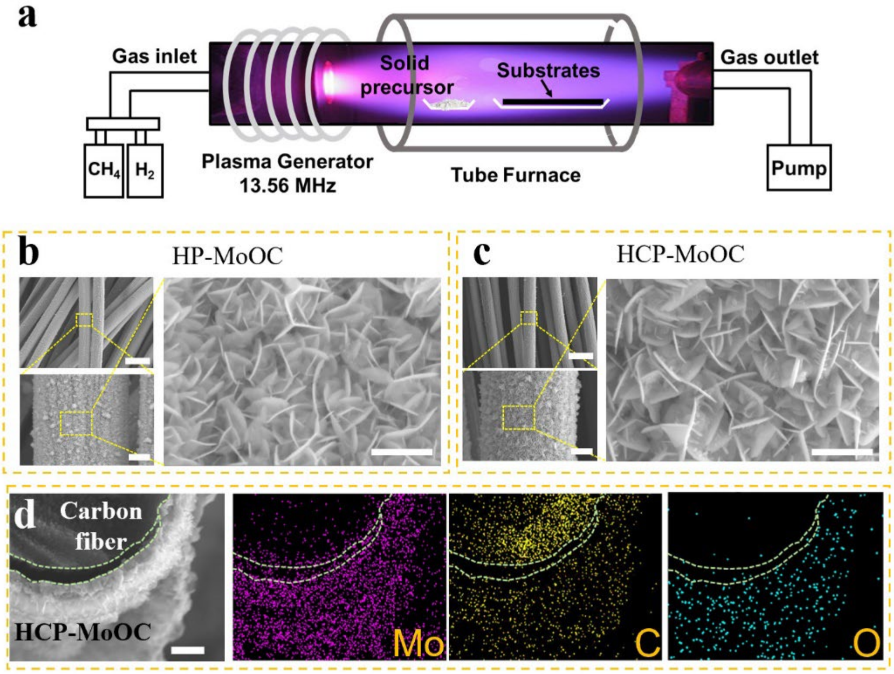

Figure 1. (a) Schematic showing the MoO_xC_y synthesized by PECVD using salts as solid precursors. SEM images of (b) HP-MoOC and (c) HCP-MoOC. Scale bars: 20 μm (top left), 2 μm (bottom left), and 500 nm (right). (d) Cross-sectional SEM image and elemental mappings of the HCP-MoOC. Scale bar: 1 μm.

Atomic structure analysis

Further investigations on the atomic structures of the PECVD-grown MoO_xC_y electrocatalysts were conducted using high-resolution transmission electron microscopy (HRTEM) and fast Fourier transform (FFT) analyses (Figure 2a and Supplementary Figure S6). These results reveal clearly that both HP-MoOC and HCP-MoOC possess a monoclinic crystalline structure. Notably, compared to HP-MoOC (Supplementary Figure S6), HCP-MoOC exhibits a carbon-encapsuled crystalline structure, where the crystalline MoO_xC_y is covered by a thin layer of carbon with a thickness of ~ 1.7 nm, as shown in Figure 2a. Additionally, the lattice spacings in HCP-MoOC are different from those in HP-MoOC, suggesting the incorporation of more carbon atoms into the crystalline structure during the methane plasma treatment. The presence of this carbon layer was also confirmed by Raman spectroscopy. As shown in Figure 2b, HCP-MoOC exhibited distinct D-band ($\omega_D \sim 1350\ \mathrm{cm}^{-1}$) and G-band ($\omega_G \sim 1584\ \mathrm{cm}^{-1}$) peaks, indicating the formation of a carbon structure[33]. In contrast, these peaks are absent in HP-MoOC, implying that the carbon layer forms only during the methane plasma treatment. X-ray diffraction (XRD) patterns of the PECVD-grown catalysts further confirm the incorporation of carbon into the lattice structure of HP-MoOC (Figure 2c). The peak of HP-MoO_2 at $2\theta = \sim 36.9°$, which corresponds to the monoclinic crystalline MoO_2 (PDF Card No. 00-032-0671)[34], shows a gradual shift toward larger values of 37.1° and 37.3° for HP-MoOC and HCP-MoOC, respectively. This noticeable peak shift can be attributed to the decreased lattice spacing as more carbon atoms are introduced into the structure.

X-ray photoelectron spectroscopy (XPS) was employed to analyze the metal valence states and electronic structures of HP-MoOC and HCP-MoOC catalysts. As displayed in Figure 2d, the Mo $3d$ spectra for both HCP-MoOC and HP-MoOC are decomposed into $3d_{5/2}$ and $3d_{3/2}$ peaks because of the spin-orbital coupling feature[35]. For both catalysts, four valence states of Mo (Mo^{2+}, Mo^{3+}, Mo^{4+}, and Mo^{6+}) are observed. The presence of Mo^{4+} originates from the atomic structure of MoO_2, while the Mo^{2+} and Mo^{3+} peaks suggest that carbon atoms are integrated into the lattice of MoO_2, therefore reducing the oxidation state of Mo. Notably, the atomic percentage of Mo^{2+} in HCP-MoOC (39.80%) is higher than that in HP-MoOC (27.46%), indicating a greater degree of chemical bonding between carbon atoms and Mo in HCP-MoOC. The peaks at 232.2 eV and 235.9 eV are the typical features of Mo^{6+}, which arise from the mild surface oxidation of the Mo-based materials when exposed to air[36,37]. To further delineate the local coordination structure of the PECVD-grown MoO_xC_y electrocatalysts, X-ray absorption near-edge structure (XANES) at the Mo K-edge were performed. The pre-edge features of both HP-MoOC and HCP-MoOC show a notable shift to lower energies compared to commercial MoO_2 powders, indicating an increased average electron density around Mo atoms due to the existence of Mo-C bonding in the MoO_xC_y. This shift is more pronounced in HCP-MoOC than in HP-MoOC, consistent with the XPS results and confirming the effect of carbon integration into the lattice structure.

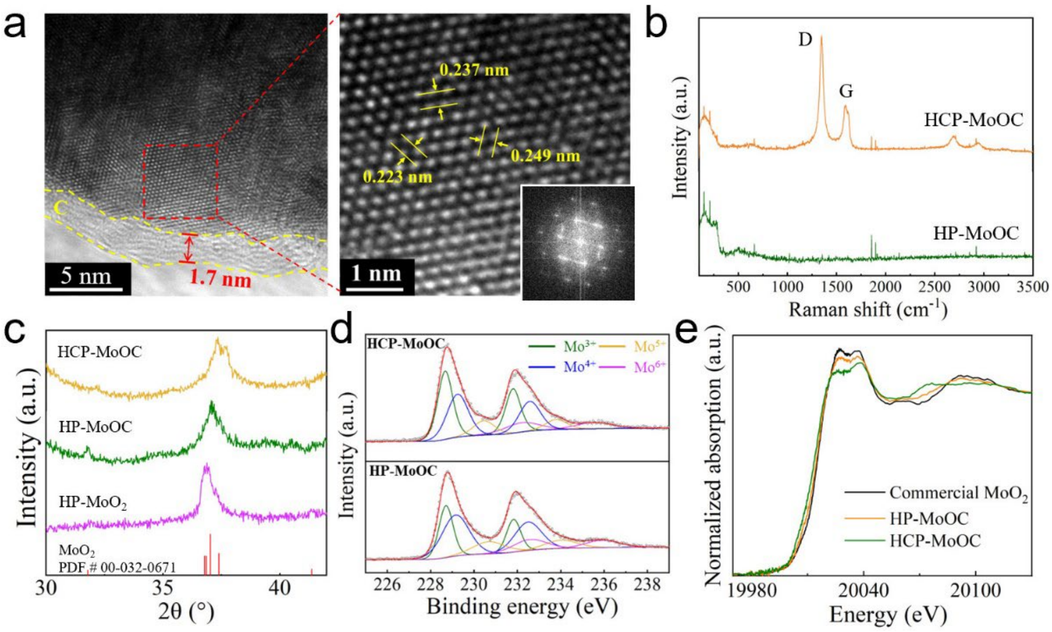

Figure 2. (a) HRTEM image of HCP-MoOC with the corresponding FFT pattern in the inset. (b) Raman spectrum of HCP-MoOC and HP-MoOC. (c) XRD spectra of HCP-MoOC, HP-MoOC, and HP-MoO_2. (d) Mo 3*d* XPS spectra of HP-MoOC and HCP-MoOC. (e) Mo K-edge XANES spectra of Mo-based samples.

HER activity evaluation

HER electrocatalytic activities of the plasma-grown catalysts were evaluated using a three-electrode electrochemical configuration in a 0.5 M H_2SO_4 electrolyte. Figure 3a shows that the plasma-grown MoO_xC_y catalysts significantly outperform the commercial MoO_2 powders, and HCP-MoOC shows superior electrocatalytic performance to that of HP-MoOC. Notably, the overpotentials (η) of both HP-MoOC and HCP-MoOC catalysts surpass those of the most widely used commercial noble Pt/C catalyst at large current densities (j >1 A cm^{-2}). Specifically, the η values for HCP-MoOC at current densities of 5 A cm^{-2} and 10 A cm^{-2} are 358 mV and 415 mV, respectively, lower than those of the existing advanced acidic HER catalysts[12,38–40], as shown in Figure 3b. The relationship between current density and the ratio of overpotential change to logarithmic current density change ($\Delta\eta/\Delta\log|j|$) of different catalysts is analyzed and shown in Figure 3c. This metric is a critical indicator of the electrocatalysts' performance at high current densities, which is essential for practical hydrogen evolution applications[41,42]. While the $\Delta\eta/\Delta\log|j|$ ratio of the Pt/C catalyst increases sharply with current density, those of HP-MoOC and HCP-MoOC maintain lower values, suggesting their superior performance at higher current densities. Notably, the $\Delta\eta/\Delta\log|j|$ ratios for HCP-MoOC are kept smaller than those for HP-MoOC at all current densities, indicating the superior electrocatalytic performance of HCP-MoOC to HP-MoOC.

The outstanding HER performance of the HCP-MoOC catalysts at high current densities can be attributed to three factors: (i) Weakened hydrogen adsorption free energy (ΔG_{H*}). The outstanding electrocatalytic performance can be evidenced by density functional theory (DFT) calculations. Atomic models were constructed for a series of Mo-based compounds including MoO_2, MoOC, Mo_2C, and Mo_2C/MoO_2 (Supplementary Figure S6) to reflect different phases of Mo-based compounds under different plasma treatment conditions. Subsequently, the ΔG_{H^*} at the Mo sites were calculated based on these models. As illustrated in Figure 3d, molybdenum oxycarbide exhibited the optimal ΔG_{H^*} (i.e., closest to 0 eV) among the four catalysts, indicating the optimal binding with hydrogen atoms and thus better HER activity of molybdenum oxycarbide compared to other catalysts. (ii) Strong localized electric field. Our prior work shows that strong local electric field can be generated near the ultrasharp edges[43], which facilitates the diffusion of H_3O^+ ions from the electrolyte to the active sites. This can effectively compensate for the rapid consumption of H_3O^+ and thus maintain HER efficiency at high current densities. (iii) Efficient H_2 bubble release. The unique vertically standing petal-like morphology of HCP-MoOC reduces the interfacial adhesion to hydrogen bubbles, enabling the rapid detachment of generated H_2 at high current densities. As shown in Figure 3e, hydrogen bubbles generated on the Pt/C surface adhere strongly and grow to a large size, covering many active sites and thereby hindering subsequent catalytic activities. In contrast, smaller hydrogen bubbles are observed on the HCP-MoOC and can be released quickly from the catalyst surface, leading to the timely exposure of catalytic sites to the surrounding electrolyte for HER at high current densities.

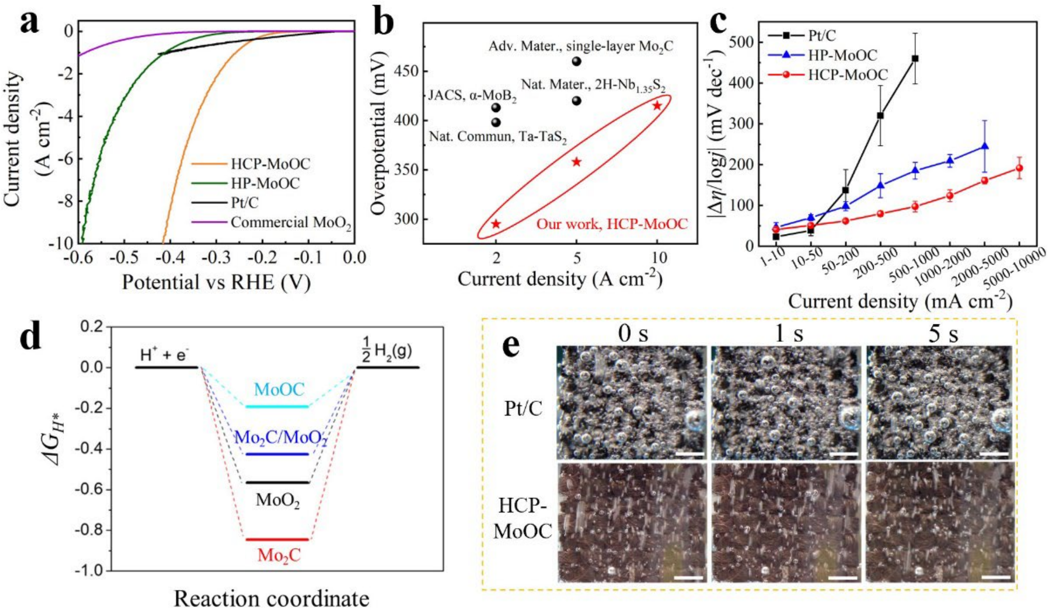

Figure 3. (a) Polarization curves of HCP-MoOC, HP-MoOC, and the commercial Pt/C and MoO_2 catalysts. (b) Comparison between the overpotential of the HCP-MoOC and the state-of-the-art catalysts. (c) $\Delta\eta/\Delta\log|j|$ ratio for Pt/C, HP-MoOC, and HCP-MoOC in different current density ranges, serving as an indicator to evaluate the electrocatalytic performance at high current densities. (d) DFT-calculated Gibbs free energy (ΔG_{H^*}) variations for HER on MoO_2, MoOC, Mo_2C, and Mo_2C/MoO_2. (e) Bubble evolution of Pt/C and HCP-MoOC catalysts at a current density of 100 mA cm^{-2}.

Long-term HER performance

The stability of the HCP-MoOC catalyst was tested using chronoamperometric (*j*-*t*) method at an ultrahigh current density of 10 A cm^{-2} (Figure 4a). The HCP-MoOC catalyst demonstrated exceptional long-term stability in 0.5 M H_2SO_4 during the HER tests, with negligible degradation over 1,000 h. This performance exceeds the aggressive target proposed by the U.S. DOE[4]. In contrast, the commercial Pt/C catalysts displayed notable degradation during the chronoamperometry test, with the performance decreased by 28% in 12 h even at a much lower current density of approximately 1 A cm^{-2}. Moreover, the polarization curve of HCP-MoOC showed a negligible shift after 10,000 cyclic voltammetry (CV) cycles (Figure

4b), suggesting its excellent durability under acidic HER conditions. The H_2 throughput of HCP-MoOC is calculated and compared with those of previously reported electrocatalysts. As shown in Figure 4c, an ultrahigh throughput of hydrogen production of up to 4,477.4 L cm^{-2} was achieved by the HCP-MoOC at an ultrahigh generation rate, significantly surpassing those of state-of-the-art HER catalysts. To further understand the ultrastable electrocatalytic performance of HCP-MoOC, the binding energy between the metal atom and adjacent atoms in the Mo-based catalysts was calculated, as shown in Figures 4d and 4e. This analysis is crucial to assessing the lattice stability, which plays a vital role in combating electrochemical decomposition and maintaining long-term HER performance at high current densities. The introduction of carbon atoms into the lattice of MoO_2 increases the binding energy from 1.4 eV to 1.7 eV, which contributes to the improved stability of the catalyst under such harsh operational conditions.

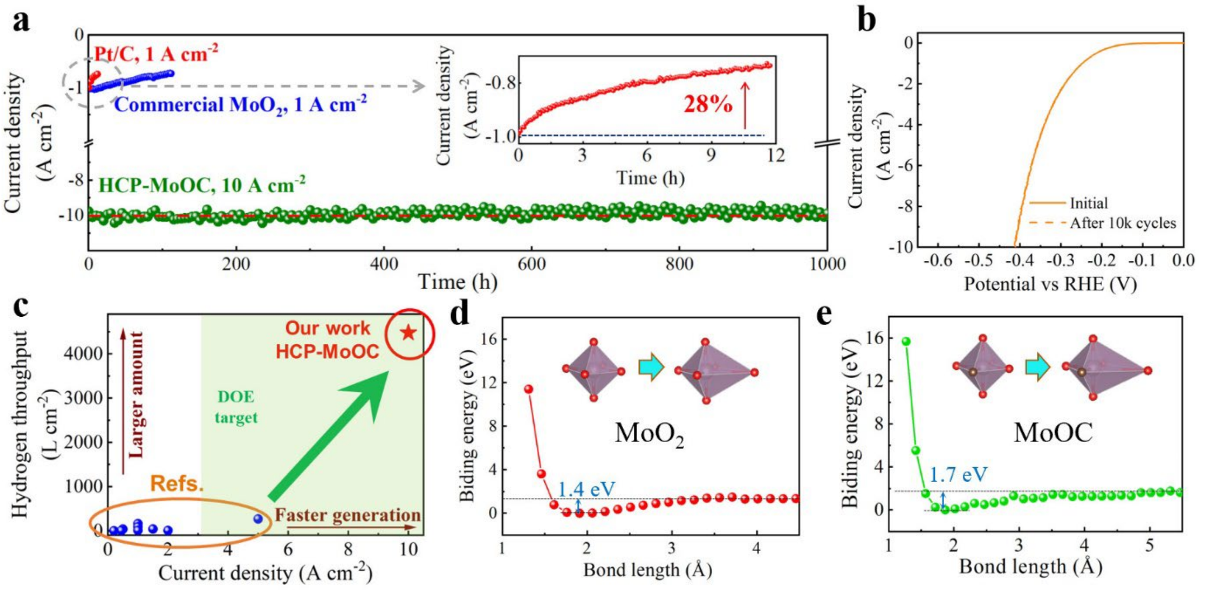

Figure 4. (a) Chronoamperometry measurements of HCP-MoOC, commercial Pt/C and MoO_2 catalysts. (b) Polarization curves of HCP-MoOC before and after 10,000 cycles. (c) Comparison between the HER

performance of the HCP-MoOC and the state-of-the-art catalysts. Calculated binding energy of (d) MoO_2 and (e) MoOC.

Conclusion

In summary, we report the design of a new catalyst based on molybdenum oxycarbide (i.e., MoO_xC_y) nanosheets with petal-like structures and controlled chemical compositions by PECVD using salts as solid precursors. The plasma-grown, nanoedge-enriched MoO_xC_y exhibits excellent acidic HER performance with a low overpotential of 415 mV at an ultrahigh current density of up to 10 A cm^{-2} for 1,000 h. As a result, an ultrahigh H_2 throughput of 4,477.4 L cm^{-2} is achieved, substantially surpassing the performance of state-of-the-art transition metal- and even noble metal-based catalysts. This work opens new avenues for the development of innovative catalysts suited for practical industrial electrocatalytic hydrogen evolution.

Acknowledgements

G.X. thanks the University of Texas at Dallas startup fund. This research used resources 7BM of the National Synchrotron Light Source II, a U.S. Department of Energy (DOE) Office of Science User Facility operated for the DOE Office of Science by Brookhaven National Laboratory under Contract No. DE-SC0012704. The authors thank Dr. Siyu Tian and Ruda Jian for their assistance in sample preparation.

Notes

The authors declare no conflicts of interest.

References

(1) Wang, Z.-J.; Li, M.-X.; Yu, J.-H.; Ge, X.-B.; Liu, Y.-H.; Wang, W.-H. Low-Iridium-Content IrNiTa Metallic Glass Films as Intrinsically Active Catalysts for Hydrogen Evolution Reaction. *Advanced Materials* **2020**, *32* (4), 1906384. https://doi.org/10.1002/adma.201906384.

(2) Cheng, L.; Huang, W.; Gong, Q.; Liu, C.; Liu, Z.; Li, Y.; Dai, H. Ultrathin WS2 Nanoflakes as a High-Performance Electrocatalyst for the Hydrogen Evolution Reaction. *Angewandte Chemie International Edition* **2014**, *53* (30), 7860–7863. https://doi.org/10.1002/anie.201402315.

(3) Zhu, Y.; Lin, Q.; Zhong, Y.; Tahini, H. A.; Shao, Z.; Wang, H. Metal Oxide-Based Materials as an Emerging Family of Hydrogen Evolution Electrocatalysts. *Energy Environ. Sci.* **2020**, *13* (10), 3361–3392. https://doi.org/10.1039/D0EE02485F.

(4) *Open Energy Data*. Energy.gov. https://www.energy.gov/data/open-energy-data (accessed 2024-05-07).

(5) Han, N.; Yang, K. R.; Lu, Z.; Li, Y.; Xu, W.; Gao, T.; Cai, Z.; Zhang, Y.; Batista, V. S.; Liu, W.; Sun, X. Nitrogen-Doped Tungsten Carbide Nanoarray as an Efficient Bifunctional Electrocatalyst for Water Splitting in Acid. *Nat Commun* **2018**, *9* (1), 924. https://doi.org/10.1038/s41467-018-03429-z.

(6) J. Kucernak, A. R.; Sundaram, V. N. N. Nickel Phosphide: The Effect of Phosphorus Content on Hydrogen Evolution Activity and Corrosion Resistance in Acidic Medium. *Journal of Materials Chemistry A* **2014**, *2* (41), 17435–17445. https://doi.org/10.1039/C4TA03468F.

(7) Zheng, Z.; Yu, L.; Gao, M.; Chen, X.; Zhou, W.; Ma, C.; Wu, L.; Zhu, J.; Meng, X.; Hu, J.; Tu, Y.; Wu, S.; Mao, J.; Tian, Z.; Deng, D. Boosting Hydrogen Evolution on MoS2 via Co-Confining Selenium in Surface and Cobalt in Inner Layer. *Nat Commun* **2020**, *11* (1), 3315. https://doi.org/10.1038/s41467-020-17199-0.

(8) Zhai, W.; Ma, Y.; Chen, D.; Ho, J. C.; Dai, Z.; Qu, Y. Recent Progress on the Long-Term Stability of Hydrogen Evolution Reaction Electrocatalysts. *InfoMat* **2022**, *4* (9), e12357. https://doi.org/10.1002/inf2.12357.

(9) Wang, Z.; Zheng, Y.-R.; Montoya, J.; Hochfilzer, D.; Cao, A.; Kibsgaard, J.; Chorkendorff, I.; Nørskov, J. K. Origins of the Instability of Nonprecious Hydrogen Evolution Reaction Catalysts at Open-Circuit Potential. *ACS Energy Lett.* **2021**, *6* (6), 2268–2274. https://doi.org/10.1021/acsenergylett.1c00876.

(10) Tsounis, C.; Subhash, B.; Kumar, P. V.; Bedford, N. M.; Zhao, Y.; Shenoy, J.; Ma, Z.; Zhang, D.; Toe, C. Y.; Cheong, S.; Tilley, R. D.; Lu, X.; Dai, L.; Han, Z.; Amal, R. Pt Single Atom Electrocatalysts at Graphene Edges for Efficient Alkaline Hydrogen Evolution. *Advanced Functional Materials* **2022**, *32* (38), 2203067. https://doi.org/10.1002/adfm.202203067.

(11) Jin, M.; Zhang, X.; Niu, S.; Wang, Q.; Huang, R.; Ling, R.; Huang, J.; Shi, R.; Amini, A.; Cheng, C. Strategies for Designing High-Performance Hydrogen Evolution Reaction Electrocatalysts at Large Current Densities above 1000 mA Cm–2. *ACS Nano* **2022**, *16* (8), 11577–11597. https://doi.org/10.1021/acsnano.2c02820.

(12) Yang, J.; Mohmad, A. R.; Wang, Y.; Fullon, R.; Song, X.; Zhao, F.; Bozkurt, I.; Augustin, M.; Santos, E. J. G.; Shin, H. S.; Zhang, W.; Voiry, D.; Jeong, H. Y.; Chhowalla, M. Ultrahigh-Current-Density Niobium Disulfide Catalysts for Hydrogen Evolution. *Nat. Mater.* **2019**, *18* (12), 1309–1314. https://doi.org/10.1038/s41563-019-0463-8.

(13) Zhang, C.; Luo, Y.; Tan, J.; Yu, Q.; Yang, F.; Zhang, Z.; Yang, L.; Cheng, H.-M.; Liu, B. High-Throughput Production of Cheap Mineral-Based Two-Dimensional Electrocatalysts for High-Current-

Density Hydrogen Evolution. *Nat Commun* **2020**, *11* (1), 3724. https://doi.org/10.1038/s41467-020-17121-8.

(14) Yao, Y.; Zhu, Y.; Pan, C.; Wang, C.; Hu, S.; Xiao, W.; Chi, X.; Fang, Y.; Yang, J.; Deng, H.; Xiao, S.; Li, J.; Luo, Z.; Guo, Y. Interfacial Sp C–O–Mo Hybridization Originated High-Current Density Hydrogen Evolution. *J. Am. Chem. Soc.* **2021**, *143* (23), 8720–8730. https://doi.org/10.1021/jacs.1c02831.

(15) Park, S.; Liu, L.; Demirkır, Ç.; Van Der Heijden, O.; Lohse, D.; Krug, D.; Koper, M. T. M. Solutal Marangoni Effect Determines Bubble Dynamics during Electrocatalytic Hydrogen Evolution. *Nat. Chem.* **2023**, *15* (11), 1532–1540. https://doi.org/10.1038/s41557-023-01294-y.

(16) Xiong, W.; Yin, H.; Wu, T.; Li, H. Challenges and Opportunities of Transition Metal Oxides as Electrocatalysts. *Chemistry – A European Journal* **2023**, *29* (5), e202202872. https://doi.org/10.1002/chem.202202872.

(17) Al-Naggar, A. H.; Shinde, N. M.; Kim, J.-S.; Mane, R. S. Water Splitting Performance of Metal and Non-Metal-Doped Transition Metal Oxide Electrocatalysts. *Coordination Chemistry Reviews* **2023**, *474*, 214864. https://doi.org/10.1016/j.ccr.2022.214864.

(18) Sher Shah, Md. S. A.; Jang, G. Y.; Zhang, K.; Park, J. H. Transition Metal Carbide-Based Nanostructures for Electrochemical Hydrogen and Oxygen Evolution Reactions. *EcoEnergy* **2023**, *1* (2), 344–374. https://doi.org/10.1002/ece2.18.

(19) Oh, Y.; Theerthagiri, J.; Min, A.; Moon, C. J.; Yu, Y.; Choi, M. Y. Pulsed Laser Interference Patterning of Transition-Metal Carbides for Stable Alkaline Water Electrolysis Kinetics. *Carbon Energy n/a* (n/a), e448. https://doi.org/10.1002/cey2.448.

(20) Wang, H.; Xu, J.; Zhang, Q.; Hu, S.; Zhou, W.; Liu, H.; Wang, X. Super-Hybrid Transition Metal Sulfide Nanoarrays of Co3S4 Nanosheet/P-Doped WS2 Nanosheet/Co9S8 Nanoparticle with Pt-Like Activities for Robust All-pH Hydrogen Evolution. *Advanced Functional Materials* **2022**, *32* (17), 2112362. https://doi.org/10.1002/adfm.202112362.

(21) Wang, M.; Zhang, L.; He, Y.; Zhu, H. Recent Advances in Transition-Metal-Sulfide-Based Bifunctional Electrocatalysts for Overall Water Splitting. *Journal of Materials Chemistry A* **2021**, *9* (9), 5320–5363. https://doi.org/10.1039/D0TA12152E.

(22) Witvrouwen, T.; Paulussen, S.; Sels, B. The Use of Non-Equilibrium Plasmas for the Synthesis of Heterogeneous Catalysts. *Plasma Processes and Polymers* **2012**, *9* (8), 750–760. https://doi.org/10.1002/ppap.201200004.

(23) Neyts, E. C.; Ostrikov, K. (Ken); Sunkara, M. K.; Bogaerts, A. Plasma Catalysis: Synergistic Effects at the Nanoscale. *Chem. Rev.* **2015**, *115* (24), 13408–13446. https://doi.org/10.1021/acs.chemrev.5b00362.

(24) Wang, Z.; Zhang, Y.; Neyts, E. C.; Cao, X.; Zhang, X.; Jang, B. W.-L.; Liu, C. Catalyst Preparation with Plasmas: How Does It Work? *ACS Catal.* **2018**, *8* (3), 2093–2110. https://doi.org/10.1021/acscatal.7b03723.

(25) Bogaerts, A.; Tu, X.; Whitehead, J. C.; Centi, G.; Lefferts, L.; Guaitella, O.; Azzolina-Jury, F.; Kim, H.-H.; Murphy, A. B.; Schneider, W. F.; Nozaki, T.; Hicks, J. C.; Rousseau, A.; Thevenet, F.; Khacef, A.; Carreon, M. The 2020 Plasma Catalysis Roadmap. *J. Phys. D: Appl. Phys.* **2020**, *53* (44), 443001. https://doi.org/10.1088/1361-6463/ab9048.

(26) Zhou, J.; Lin, J.; Huang, X.; Zhou, Y.; Chen, Y.; Xia, J.; Wang, H.; Xie, Y.; Yu, H.; Lei, J.; Wu, D.; Liu, F.; Fu, Q.; Zeng, Q.; Hsu, C.-H.; Yang, C.; Lu, L.; Yu, T.; Shen, Z.; Lin, H.; Yakobson, B. I.; Liu, Q.; Suenaga, K.; Liu, G.; Liu, Z. A Library of Atomically Thin Metal Chalcogenides. *Nature* **2018**, *556*

(7701), 355–359. https://doi.org/10.1038/s41586-018-0008-3.

(27) Li, S.; Lin, Y.-C.; Hong, J.; Gao, B.; Lim, H. E.; Yang, X.; Liu, S.; Tateyama, Y.; Tsukagoshi, K.; Sakuma, Y.; Suenaga, K.; Taniguchi, T. Mixed-Salt Enhanced Chemical Vapor Deposition of Two-Dimensional Transition Metal Dichalcogenides. *Chem. Mater.* **2021**, *33* (18), 7301–7308. https://doi.org/10.1021/acs.chemmater.1c01652.

(28) Tang, L.; Tan, J.; Nong, H.; Liu, B.; Cheng, H.-M. Chemical Vapor Deposition Growth of Two-Dimensional Compound Materials: Controllability, Material Quality, and Growth Mechanism. *Acc. Mater. Res.* **2021**, *2* (1), 36–47. https://doi.org/10.1021/accountsmr.0c00063.

(29) Wu, S.; Huang, D.; Yu, H.; Tian, S.; Malik, A.; Luo, T.; Xiong, G. Molecular Understanding of the Effect of Hydrogen on Graphene Growth by Plasma-Enhanced Chemical Vapor Deposition. *Phys. Chem. Chem. Phys.* **2022**, *24* (17), 10297–10304. https://doi.org/10.1039/D1CP04510E.

(30) Zhang, H.; Cao, T.; Cheng, Y. Preparation of Few-Layer Graphene Nanosheets by Radio-Frequency Induction Thermal Plasma. *Carbon* **2015**, *86*, 38–45. https://doi.org/10.1016/j.carbon.2015.01.021.

(31) Han, Z. J.; Murdock, A. T.; Seo, D. H.; Bendavid, A. Recent Progress in Plasma-Assisted Synthesis and Modification of 2D Materials. *2D Mater.* **2018**, *5* (3), 032002. https://doi.org/10.1088/2053-1583/aabb81.

(32) Li, S. Salt-Assisted Chemical Vapor Deposition of Two-Dimensional Transition Metal Dichalcogenides. *iScience* **2021**, *24* (11), 103229. https://doi.org/10.1016/j.isci.2021.103229.

(33) Ferrari, A. C.; Basko, D. M. Raman Spectroscopy as a Versatile Tool for Studying the Properties of Graphene. *Nature Nanotech* **2013**, *8* (4), 235–246. https://doi.org/10.1038/nnano.2013.46.

(34) Zhang, Q.; Li, X.; Ma, Q.; Zhang, Q.; Bai, H.; Yi, W.; Liu, J.; Han, J.; Xi, G. A Metallic Molybdenum Dioxide with High Stability for Surface Enhanced Raman Spectroscopy. *Nat Commun* **2017**, *8* (1), 14903. https://doi.org/10.1038/ncomms14903.

(35) Wu, X.; Wang, Z.; Zhang, D.; Qin, Y.; Wang, M.; Han, Y.; Zhan, T.; Yang, B.; Li, S.; Lai, J.; Wang, L. Solvent-Free Microwave Synthesis of Ultra-Small Ru-Mo2C@CNT with Strong Metal-Support Interaction for Industrial Hydrogen Evolution. *Nat Commun* **2021**, *12* (1), 4018. https://doi.org/10.1038/s41467-021-24322-2.

(36) Liu, Y.; Huang, B.; Xie, Z. Hydrothermal Synthesis of Core-Shell MoO2/α-Mo2C Heterojunction as High Performance Electrocatalyst for Hydrogen Evolution Reaction. *Applied Surface Science* **2018**, *427*, 693–701. https://doi.org/10.1016/j.apsusc.2017.08.098.

(37) Yang, H.; Chen, X.; Hu, G.; Chen, W.-T.; J. Bradley, S.; Zhang, W.; Verma, G.; Nann, T.; Jiang, D.; E. Kruger, P.; Wang, X.; Tian, H.; N. Waterhouse, G. I.; G. Telfer, S.; Ma, S. Highly Efficient Electrocatalytic Hydrogen Evolution Promoted by O–Mo–C Interfaces of Ultrafine β-Mo 2 C Nanostructures. *Chemical Science* **2020**, *11* (13), 3523–3530. https://doi.org/10.1039/D0SC00427H.

(38) Cheng, X.; Li, Y.; Zheng, L.; Yan, Y.; Zhang, Y.; Chen, G.; Sun, S.; Zhang, J. Highly Active, Stable Oxidized Platinum Clusters as Electrocatalysts for the Hydrogen Evolution Reaction. *Energy & Environmental Science* **2017**, *10* (11), 2450–2458. https://doi.org/10.1039/C7EE02537H.

(39) Wu, J.; Su, J.; Wu, T.; Huang, L.; Li, Q.; Luo, Y.; Jin, H.; Zhou, J.; Zhai, T.; Wang, D.; Gogotsi, Y.; Li, Y. Scalable Synthesis of 2D Mo2C and Thickness-Dependent Hydrogen Evolution on Its Basal Plane and Edges. *Advanced Materials* **2023**, *35* (25), 2209954. https://doi.org/10.1002/adma.202209954.

(40) Yu, Q.; Zhang, Z.; Qiu, S.; Luo, Y.; Liu, Z.; Yang, F.; Liu, H.; Ge, S.; Zou, X.; Ding, B.; Ren, W.; Cheng, H.-M.; Sun, C.; Liu, B. A Ta-TaS2 Monolith Catalyst with Robust and Metallic Interface for Superior Hydrogen Evolution. *Nat Commun* **2021**, *12* (1), 6051. https://doi.org/10.1038/s41467-021-26315-7.

(41) Yang, L.; Wang, D.; Liu, M.; Liu, H.; Tan, J.; Wang, Z.; Zhou, H.; Yu, Q.; Wang, J.; Lin, J.; Zou, X.; Qiu, L.; Cheng, H.-M.; Liu, B. Glue-Assisted Grinding Exfoliation of Large-Size 2D Materials for Insulating Thermal Conduction and Large-Current-Density Hydrogen Evolution. *Materials Today* **2021**, *51*, 145–154. https://doi.org/10.1016/j.mattod.2021.08.009.

(42) Luo, Y.; Tang, L.; Khan, U.; Yu, Q.; Cheng, H.-M.; Zou, X.; Liu, B. Morphology and Surface Chemistry Engineering toward pH-Universal Catalysts for Hydrogen Evolution at High Current Density. *Nat Commun* **2019**, *10* (1), 269. https://doi.org/10.1038/s41467-018-07792-9.

(43) Xiong, G.; He, P.; Lyu, Z.; Chen, T.; Huang, B.; Chen, L.; Fisher, T. S. Bioinspired Leaves-on-Branchlet Hybrid Carbon Nanostructure for Supercapacitors. *Nat Commun* **2018**, *9* (1), 790. https://doi.org/10.1038/s41467-018-03112-3.